RSC Advances

Electrochemical Properties of Layered SnO and PbO for Energy Applications

Journal:	*RSC Advances*
Manuscript ID	RA-ART-09-2015-018776.R1
Article Type:	Paper
Date Submitted by the Author:	10-Nov-2015
Complete List of Authors:	Lim, Chee Shan; Nanyang Technological University, Chemistry and Biological Chemistry Sofer, Zdenek; Institute of Chemical Technology, Prague, Department of Inorganic Chemistry Jankovský, Ondřej; Institute of Chemical Technology, Dept. of Inorganic Chemistry Wang, Hong; Nanyang Technological University, Division of Chemistry and Biological Chemistry Pumera, Martin; Nanyang Technological University, Chemistry and Biological Chemistry
Subject area & keyword:	Nanomaterials - Materials < Materials

Electrochemical Properties of Layered SnO and PbO for Energy Applications

Received 00th January 20xx,
Accepted 00th January 20xx

DOI: 10.1039/x0xx00000x

www.rsc.org/

Chee Shan Lim[a], Zdeněk Sofer[b], Ondřej Jankovský[b], Hong Wang[a], Martin Pumera*[a]

In this paper we synthetized four different lead oxides with tetragonal or orthorhombic symmetry either by thermal decomposition or a chemical route. Another two tin oxides were also synthesized by thermal decomposition and chemical route respectively. We analysed their structure by XRD and SEM and chemical composition by EDS and XPS. Thermal decomposition was analysed using STA. The surface areas were determined by BET. Electrochemical behavior such as heterogeneous electron transfer rate, electrocatalytic properties in hydrogen evolution and oxygen reduction reactions were also investigated by cyclic voltammetry and linear sweep voltammetry . Results suggest that studied materials are promising candidatses for catalysis or various applications in energy management .

Introduction

The group of metal oxide materials include a huge number of different substances with wide applications ranging from supercapacitors [1,2] and transistors [3] to energy storage systems.[4,5] The main advantage of these materials are their high chemical and thermal stability. Among the metal oxides, transition metal oxides (TMOs) have been intensively used for a wide spectrum of applications. For instance, copper oxide has been used for electrochemical sensing [6] and electrocatalytic purposes,[7] while zinc oxide was implemented for solar energy systems[8,9] and biosensors.[10,11] Iron, titanium and nickel oxides are also highly utilized in fields such as biomedical, [12] electrochemical water-splitting [13,14] and electrochromic devices as well.[15,16]

In recent years a very detail research on transition metal dichalcogenides has been started. It was found that molybdenum disulfide, tungsten disulfide and other structural analogues have outstanding properties in catalyzing applications such as hydrogen evolution (HER) or oxygen reduction reactions (ORR).[17,18] Similarly, layered cobalt mixed oxides have also been proposed as promising candidates for HER and ORR,[19,20,21] Due to structural similarities the study of layered oxides is also an important issue.

In our study we focused on two 14th group metal oxides, namely lead (II) and tin(II) oxide with layered structures. Tin(II) oxide, also known as stannous oxide or tin monoxide, exists in a tetragonal symmetry (space group *P*4/*nmm*).[22,23] Its structure is shown in Figure 1A. The discovery of tin(II) oxide as a p-type semiconductor in 2001, coupled with its high carrier mobility, has led to a series of development of this material as thin-film transistors.[24,25] In addition, tin(II) oxide has also been widely used in applications such as the self-assembly of nanodiskettes and lithium-ion batteries owing to its high theoretical capacities and low cost.[26,27] Preparation of tin(II) oxide by precipitation from tin chloride and urea, laser vaporisation and solvothermal methods was reported.[28,29,30]

The second studied material, lead(II) oxide, generally exist in two polymorphic forms, tetragonal (red) and orthorhombic (yellow), which are also known as litharge and massicot, respectively. Tetragonal lead(II) oxide is known to be isostructural to tin(II) oxide (Figure 1B)[31] with a layered structure. In this structure each oxygen atom is sandwiched between two lead layers. The orthorhombic form of lead(II) oxide exhibits in a space group *Pbma* (Figure 1C).[32,33] This structural type is related to the structure of black phosphorus which is isoelectronic with lead(II) oxide. Both forms of lead(II) oxide can be prepared using thermal decomposition of lead(II) salts such as lead(II) carbonate.[34] In terms of thermal stability, the tetragonal lead(II) oxide is stable at lower temperatures, while the orthorhombic form is stable at higher temperatures.[35] Though both types of lead(II) oxide display low electrical conductivity, they possess notable photoconducting and semiconducting behaviors.[33] Lead(II) oxide has been prominent in x-ray detectors,[36] lead-acid batteries[37] and catalytic applications[38] over the years.

Lead and tin oxides have also great potential for energy applications. Lead (II) oxide and nano-lead (II) oxide were used as anodes in lithium rechargeable batteries.[39] The reversibility of Pb(II)/PbO_2 conversion was tested for its possible application in flow liquid batteries.[40] Lead (II) oxide nanoparticles were application to Pb(II)-selective electrode based on cellulose acetate.[41] On the other hand tin oxides were used in solar energy systems[42-44] Also porous tin oxide nanowire bundles were tested for photocatalyst and Li ion battery applications.[45] Hollow tin (IV) oxide was used for dye-sensitized solar cells.[46]

Despite their remarkable uses, electrochemistry of lead(II) oxide and tin(II) oxide has not been studied in detail yet. Hence, the electrochemical study of these two oxides will be undertaken in this work, including their electrocatalytic abilities in energy-related reactions such as hydrogen evolution (HER) and oxygen reduction (ORR). Compare to precious metal electrocatalysts, these material are significantly

[a] School of Physical and Mathematical Science, Division of Chemistry and Biological Chemistry, Nanyang Technological University, 21 Nanyang Link, Singapore. Email: pumera.research@gmail.com
[b] Institute of Chemical Technology, Department of Inorganic Chemistry, Technická 5, 166 28 Prague 6, Czech Republic.

more abundant and broadly available at suitable prices for large scale industrial applications.

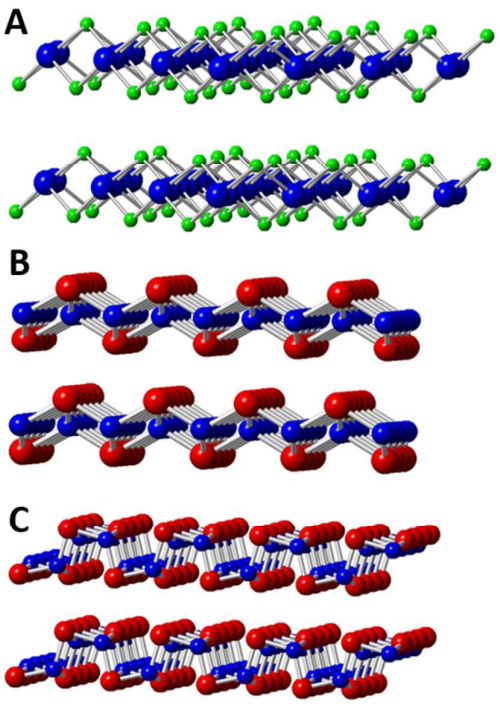

Figure 1 The structure of (A) tetragonal tin(II) oxide, (B) tetragonal lead(II) oxide and (C) orthorhombic lead(II) oxide. Legend: green – tin, red – lead, blue – oxygen.

Experimental

Materials

Tin(II) chloride dehydrate, sodium carbonate, oxalic acid dehydrate, potassium hydroxide, lead carbonate and lead nitrate were obtained from Lach-Ner, Czech Republic. Argon of 99.996% purity was obtained from SIAD, Czech Republic. Nafion 117 solution, platinum on graphitized carbon, sulfuric acid (95-98 %, v/v), potassium hydroxide, sodium chloride, potassium chloride, sodium phosphate dibasic and potassium phosphate monobasic were obtained from Sigma-Aldrich, Singapore. Glassy carbon (GC) electrodes with a diameter of 3 mm were obtained from Autolab, The Netherlands. Milli-Q water with a resistivity of 18.2 MΩ cm was used throughout the experiments.

Synthesis Procedure

The thermally-prepared lead(II) oxides were synthesized by the thermal decomposition of lead carbonate in alumina crucible at 350 °C, 400 °C, 450 °C, 500 °C, 550 °C and 600 °C for 2 hours in static air atmosphere with the heating and cooling rates 5 °C min^{-1}. Another set of experiments was performed at 400 °C and 450 °C in dynamic argon atmosphere with flow rate 50 cm^3 min^{-1} for 2 hours in static air atmosphere with the heating and cooling rates 5 °C min^{-1}.

Chemically-prepared lead oxides were synthesized using crystallization of Pb^{2+} from hot KOH of variable concentrations. 150 mL of 5 M KOH was heated on 100 °C and saturated with lead by slow addition of $Pb(NO_3)_2$. The prepared solution was placed in Dewar flask and allowed to crystallize overnight. The orthorhombic PbO crystals existed in the form of yellow plates with size up to 5 x 5 mm; the crystals were separated by suction filtration and repeatedly washed with water. The tetragonal modification was prepared in the similar way using 15 M KOH. Dark red crystals in the form of plates with size up to 1x1 mm were formed and separated by suction filtration before washing with water repeatedly.

Similarly, thermally-prepared tin(II) oxide was synthesized by the thermal decomposition of tin(II) oxalate. Tin(II) oxalate was prepared by adding 10 wt% oxalic acid to 10 wt% solution of tin(II) chloride acidified with hydrochloric acid of pH 2. The white precipitate of tin(II) oxalate formed was separated by suction filtration and repeatedly washed with water before drying in vacuum oven at 50 °C. The tin(II) oxalate was decomposed in argon atmosphere at 380 °C for 5 hours. The heating rate and cooling rate was 5 °C min^{-1}.

The chemical synthesis is based on preparation of hydrated tin(II) oxide and following dehydration. 50 ml of saturated solution of $SnCl_2.2H_2O$ in concentrated hydrochloric acid was neutralized with saturated aqueous solution of Na_2CO_3 on pH > 9. Formed suspension was heated at 110 °C for 3 hours. During the heating procedure, a white precipitate of hydrated tin(II) oxide was converted to crystalline material. Blue-black crystals were separated by suction filtration, and washed repeatedly with water before drying in vacuum oven at 50 °C for 48 hours.

Instrumentation

X-ray diffraction (XRD) was carried out on Bruker D8 Discoverer in Bragg–Brentano parafocusing geometry using CuK_α radiation, and recorded within the range 2θ = 5 - 80° to evaluate the phase composition of the materials.

Simultaneous thermal analysis (STA) was performed on a *Linseis PT 1600* from room temperature to 800 °C in an alumina crucible to study the decomposition process. The heating rate was set to 5 °C min^{-1} and measurements were carried out in a dynamic argon or air atmosphere with a flow rate of 50 mL min^{-1}.

Scanning electron microscopy (SEM) was carried out with Jeol 7600F SEM (Jeol, Japan) operating at 5 kV in GB high to investigate the morphology of the oxides.

Energy-dispersive X-ray spectroscopy (EDS) was performed on a Jeol 7600F (Jeol, Japan) at 30 kV to obtain the elemental composition and spectrum mapping of the oxides.

X-ray photoelectron spectroscopy (XPS) measurements were analysed using a Phoibos 100 spectrometer and a Mg X-ray radiation source (SPECS, Germany). Survey scans and high-resolution spectra of the oxides were measured to ascertain and compare the surface composition of the materials. Sample preparation was performed by fixing the material onto an aluminium XPS sample holder using a sticky conductive carbon tape. A uniform layer of the material was ensured throughout.

The surface area was measured using a sorption analyzer, Coulter SA 3100 (Backman Coulter). The samples were outgassed for 4 hours at 160 °C under high vacuum prior to the

sorption experiments. The reason for such low temperature is to avoid degradation and further decomposition of oxygen functionalities, present mainly in CRG, on graphene. A TCD nitrogen cooled (77 K) detector was used for the evaluation of the results using BET and Kelvin equations.

Linear sweep voltammetry (LSV) and cyclic voltammetry (CV) measurements were carried out with a µAutolab type III electrochemical analyser (Eco Chemie, The Netherlands) connected to a personal computer and controlled by NOVA 1.10 software. All experiments were performed in a 5 mL electrochemical cell using a three-electrode configuration at room temperature; a platinum electrode was used as a counter electrode while an Ag/AgCl electrode functioned as a reference electrode. All electrochemical potentials in this work are presented *vs.* the Ag/AgCl reference electrode unless otherwise stated.

Cyclic voltammetry measurements were performed using a scan rate of 100 mV s^{-1} for inherent electrochemistry scans. Linear sweep voltammetry measurements were recorded at a scan rate of 2 mVs^{-1} for HER and 5 mV s^{-1} for ORR. 0.5 M sulfuric acid was used as the electrolyte for HER, whereas 0.1 M potassium hydroxide acted as the electrolyte for ORR. Reproducibility of the measurements was obtained over three different electrode units for each experiment.

A suspension of the desired material with a concentration of 5 mg mL^{-1} in respective solvent mixtures was first prepared, followed by a 60 min ultrasonication. DMF was used as the solvent for HER; water suspension with 0.1 wt% nafion solution was used as the solvent for ORR. A micropipette was then used to deposit 1 µL aliquot of the respective suspension onto the electrode surface to immobilise the material onto the working electrode. The solvent was allowed to evaporate at room temperature to achieve an evenly distributed film on the electrode surface. To renew the electrode surfaces, polishing was done with 0.05 µm alumina powder on a polishing pad.

Results and Discussion

The lead and tin oxides were synthesized *via* the chemical and thermal methods, with the former generated in both orthorhombic and tetragonal forms. The two thermally-prepared PbO were abbreviated as PbO-R-T (tetragonal) and PbO-Y-T (orthorhombic) in this work while the two chemically-prepared PbO as PbO-R-C (tetragonal) and PbO-Y-C (orthorhombic), with the letters R and Y symbolizing the red and yellow colours of the materials, T and C denoting the synthesis methods respectively. The two tin oxides are abbreviated as SnO-T and SnO-C on the other hand, denoting the different preparation routes. Syntheses of the oxide materials were firstly optimized and characterised using X-ray diffraction (XRD).

The chemically prepared orthorhombic (PbO-Y-C) and tetragonal (PbO-R-C) lead oxides were synthesized by the crystallisation of lead(II) ions in KOH. XRD diffractograms in Figures 2A and 2B confirmed the presence of single phase samples with negligible impurities present. Subsequently, the synthesis of PbO-Y-T was optimised by varying the reaction temperatures. The decomposition of $PbCO_3$ in air at 350 °C led to the formation of tetragonal PbO (orange colour, space group *P4/nmm*, denoted by PbO-R-T)[47] with minor impurities composed of lead oxide carbonate ($PbCO_3$.2PbO), suggesting incomplete decomposition.[48]

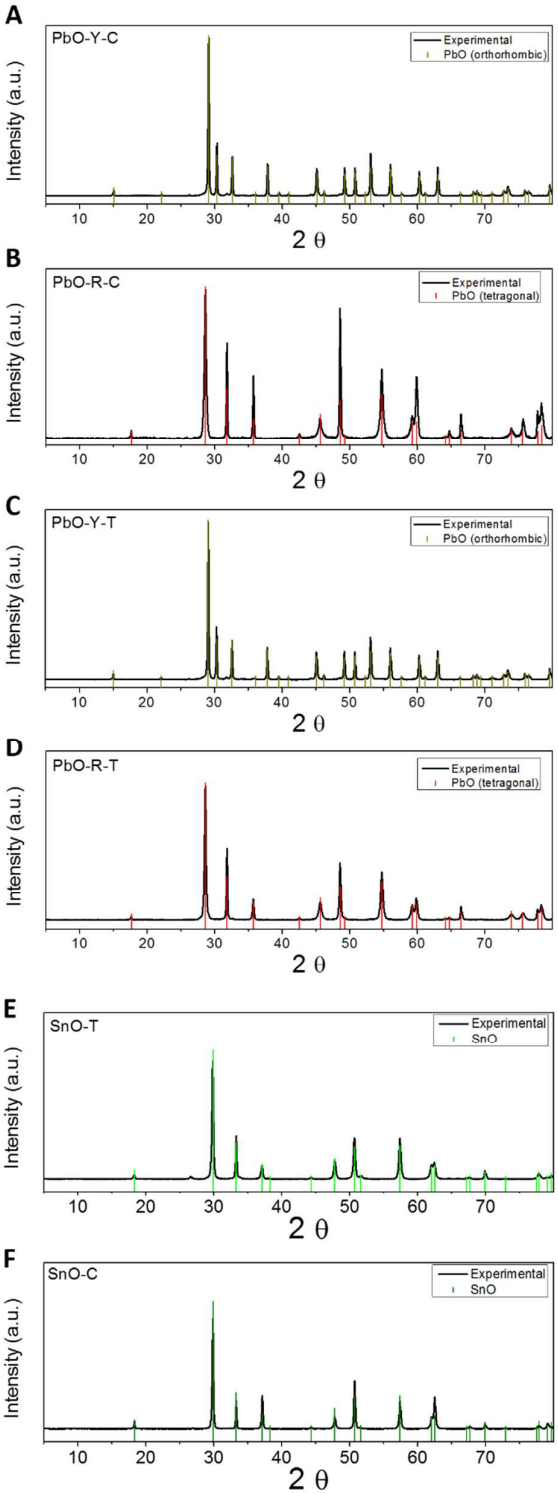

Figure 2. The X-ray diffractograms of PbO and SnO samples.

The second sample decomposed at 400 °C contained tetragonal and hexagonal Pb_3O_4 other than the expected tetragonal PbO.[49,50] In fact, the two Pb_3O_4 were present in higher amount. Sample decomposed at 450 °C contained both tetragonal PbO and Pb_3O_4, while the sample decomposed at 500 °C contained mixture of three phases: tetragonal PbO, tetragonal Pb_3O_4 and orthorhombic PbO (yellow colour, space group Pbcm).[51] Next, the sample decomposed at 550 °C contained orthorhombic PbO with small amount of tetragonal PbO and tetragonal Pb_3O_4. Finally, the sample decomposition at 600 °C in air led to formation of pure orthorhombic PbO. The X-ray diffractogram of the pure orthorhombic phase (PbO-Y-T) is shown in Figure 2C while the remaining diffractograms are displayed in SI (Figure S1). These findings indicate high tendency of Pb^{2+} oxidation and formation of Pb^{4+} at low temperatures.

To avoid the oxidation of Pb^{2+} to Pb^{4+}, the synthesis of low temperature pure tetragonal PbO (PbO-R-T) was performed by thermal decomposition of $PbCO_3$ in argon atmosphere. While the sample decomposed at 450 °C contained already secondary high temperature orthorhombic PbO, the sample decomposed at 400 °C exhibited a single phase structure and contained only tetragonal PbO. Diffractogram for the single phase sample is presented in Figure 2D, with the second XRD diffractogram shown in the SI (Figure S2). PbO-R-T was successfully synthesized as an orange-red powder.

Finally, the successful syntheses of both thermally and chemically prepared tin oxides, SnO-T and SnO-C were ascertained by XRD diffractograms displayed in Figures 2E and 2F. The X-ray diffractograms in both cases were in good agreement with that established by earlier studies,[23] as they revealed the presence of tetragonal SnO (space group P4/nmm).

Thermally-prepared oxides were then studied with simultaneous thermal analysis (STA) to comprehend their detailed syntheses. Thermal decomposition of $PbCO_3$ in both argon and air atmospheres were analysed in Figures 3A and Figure 3B. A two-step decomposition of $PbCO_3$ was established in argon atmosphere, where the first step likely involves the formation of $PbCO_3$.2PbO followed by a further decomposition to obtain tetragonal PbO, PbO-R-T. The weight loss corresponds to the decomposition of $PbCO_3$ to PbO. Surprisingly, the decomposition in air to synthesize PbO-Y-T showed very similar behaviour as that carried out in argon atmosphere. Other than the two-step decomposition from $PbCO_3$ to PbO, no other thermal implications such as oxidation of PbO to Pb_3O_4 were detected. This is probably due to the crucible with perforated lid used during the reaction which prevented carbon dioxide produced from escaping. This significantly decreases the local partial pressure of oxygen, hence disabling the oxidation of PbO.

The process of SnO-T formation was studied by the thermal decomposition of $Sn(COO)_2$ in argon atmosphere, as illustrated in Figure 3C. A large endothermic effect along with weight decrease were detected at approximately 360 °C, confirming successful synthesis of SnO. The broad exothermic effect

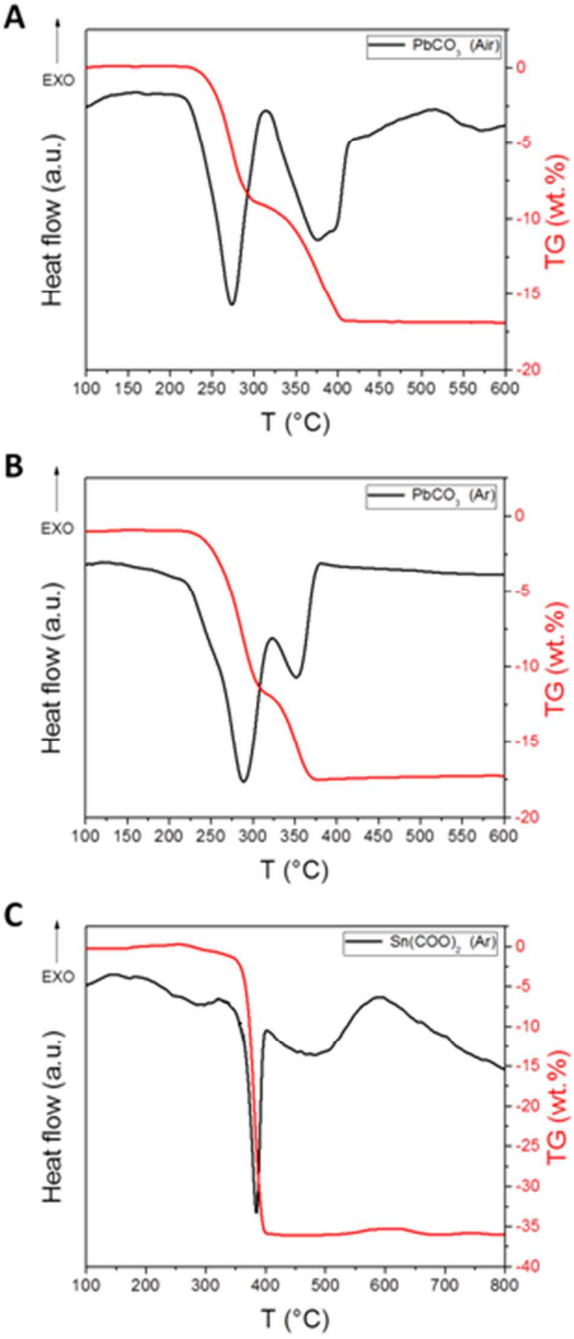

Figure 3. The STA data of thermal decomposition of (A) $PbCO_3$ in air, (B) $PbCO_3$ in argon atmosphere and (C) $Sn(COO)_2$ in argon atmosphere.

observed at higher temperatures is likely to originate from the disproportionation of SnO to Sn, SnO_2 and Sn_3O_4.

Structural and morphological comparisons were next drawn prior to obtain a clearer idea of the different forms of the oxides. Morphological studies were first performed using scanning electron microscopy (SEM), as illustrated in Figures 4 and 5. For the various forms of PbO, the chemically prepared tetragonal (Figure 4A) and orthorhombic (Figure 4C) PbO have

significantly larger particles than those prepared by thermal decomposition of lead carbonate (Figures 4B and 4D).

PbO-R-C contains large irregular particles at about 30 µm in length, with rough particle surfaces whereas PbO-Y-C existed in smooth, layered sheets of different sizes, with thickness of less than 0.1 µm. Both lead oxides prepared by carbonate thermal decomposition appeared as smaller round particles which are closely packed together, forming larger agglomerates. PbO-R-T and PbO-Y-T particles have a length of about 2 µm but PbO-Y-T show platelet-like crystal habits compared to PbO-R-T, concurring with the observation for the lead oxides prepared by crystallization from KOH solution.

Structural forms of the two SnO are presented in Figure 5, with SnO-T showing a mesh-like structure with particles interconnected together. The particles are generally round, as seen in a magnified image in Figure 5A (right), with diameters ranging from about 0.1 to 0.5 µm. Regular rectangular blocks with relatively smooth surfaces were evident for the other tin oxide sample, SnO-C as displayed in Figure 5B. The thickness of the particles is around 1 to 2 µm, indicating that the particles in SnO-C are generally bulky in size.

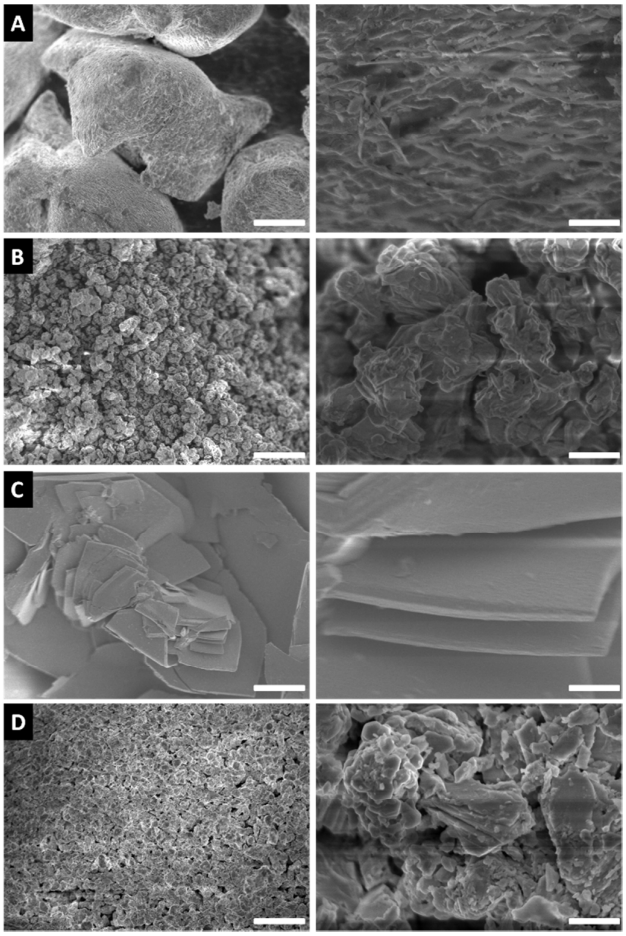

Figure 4. SEM images of (A) PbO-R-C, (B) PbO-R-T, (C) PbO-Y-C and (D) PbO-Y-T at magnifications of (left panel) 2,000 and (right panel) 20,000 x respectively. Scale bar: 10 µM (left) and 1 µM (right)

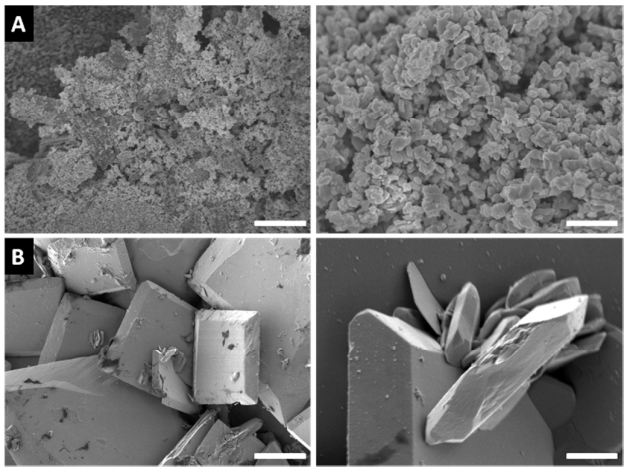

Figure 5. SEM images of (A) SnO-T and (B) SnO-C at magnifications of (left panel) 2 000x and (right panel) 20 000x respectively. Scale bar: 10 µm (left) and 1 µm (right).

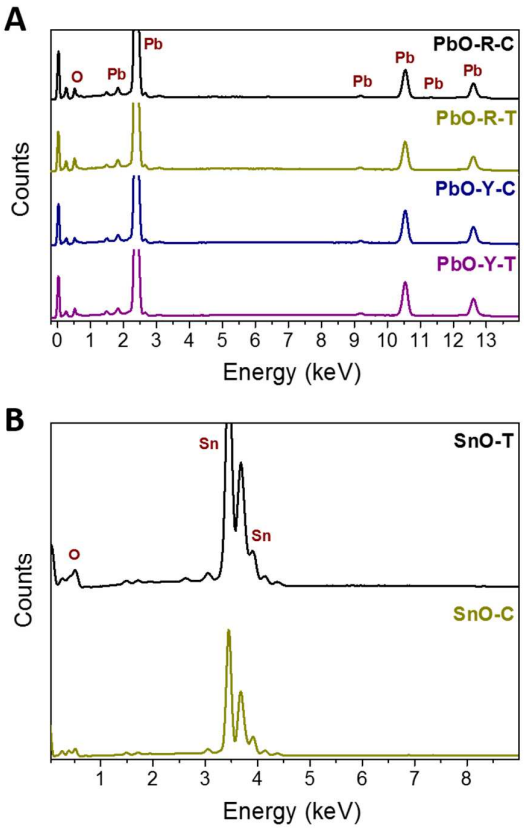

Figure 6. Energy-dispersive X-ray spectroscopy (EDX) spectra of (A) lead oxides and (B) tin oxides.

Energy-dispersive X-ray spectroscopy (EDX) was subsequently carried out to detect any impurities. EDX spectra for all four lead oxides contained identical peaks (Figure 6A) with negligible impurities present. Prominent tin and oxygen peaks were observed for the EDX spectra of the two tin oxides as well, as illustrated in Figure 6B. Similar to lead oxide only negligible concentration of impurities was detected.

Finally, X-ray photoelectron spectroscopy (XPS) was performed to detect the surface composition as well as the chemical environments in the materials. Survey scans for the lead oxide materials illustrated in Figure 7A shows prominent peaks for the two elements, lead and oxygen with little contaminants. This result is consistent for all four lead oxides. High-resolution spectra for Pb 4f are recorded in Figure 7B to compare the positions of the signals across the four lead oxides. All of them have a pair of spin-orbit coupling peaks for $4f_{7/2}$ and $4f_{5/2}$ except for PbO-Y-C, which has two pair of signals. Positions of the respective signals together with the spin-orbit splitting (δ) are summarised in Table 1. The Pb 4f signals seem to be dependent on the synthesis methods, with the thermally treated materials located at slightly lower binding energies. These values, though showing marginal discrepancies, concur largely with those obtained in previous studies. Literature values for the Pb $4f_{7/2}$ signals were reported to be about 138.0 – 138.3 eV, depending on the structure, with a δ value of around 4.8 eV.[52,53] The only anomaly arises from PbO-Y-C, where a second set of peaks was observed. This is attributed to presence of lead in another chemical environment. Despite so, the main set of peaks was still evident in PbO-Y-C. As for the O 1s spectra shown in Figure 7C, previous studies reported a signal at about 531.0 eV with traces of shoulder peaks at slight lower binding energies. The reported results in this work (Table 1) agree largely with the earlier findings, with PbO-R-C

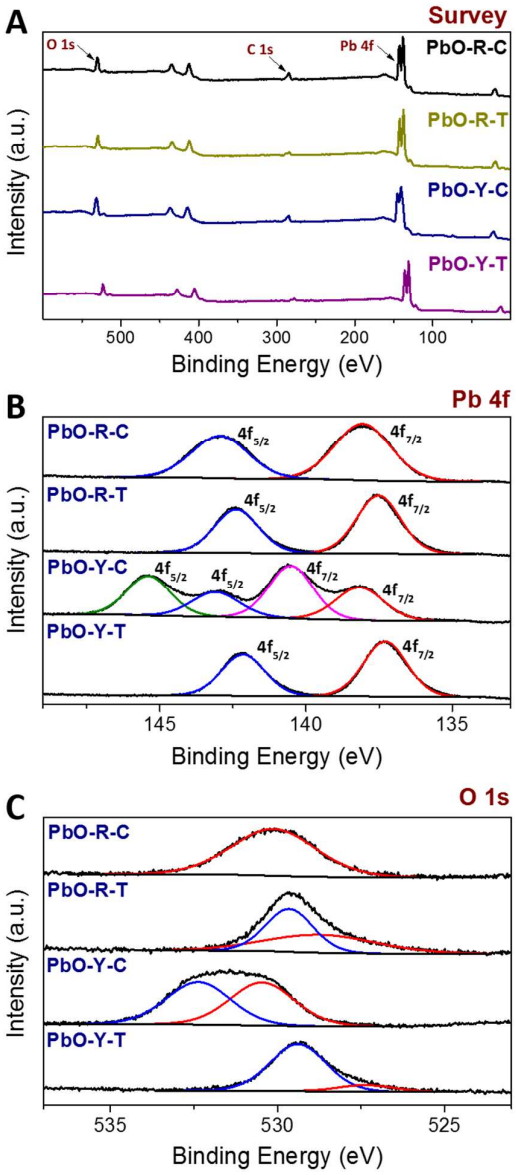

Figure 7. (A) Survey scan (top row) and (B, C) high resolution spectra of PbO.

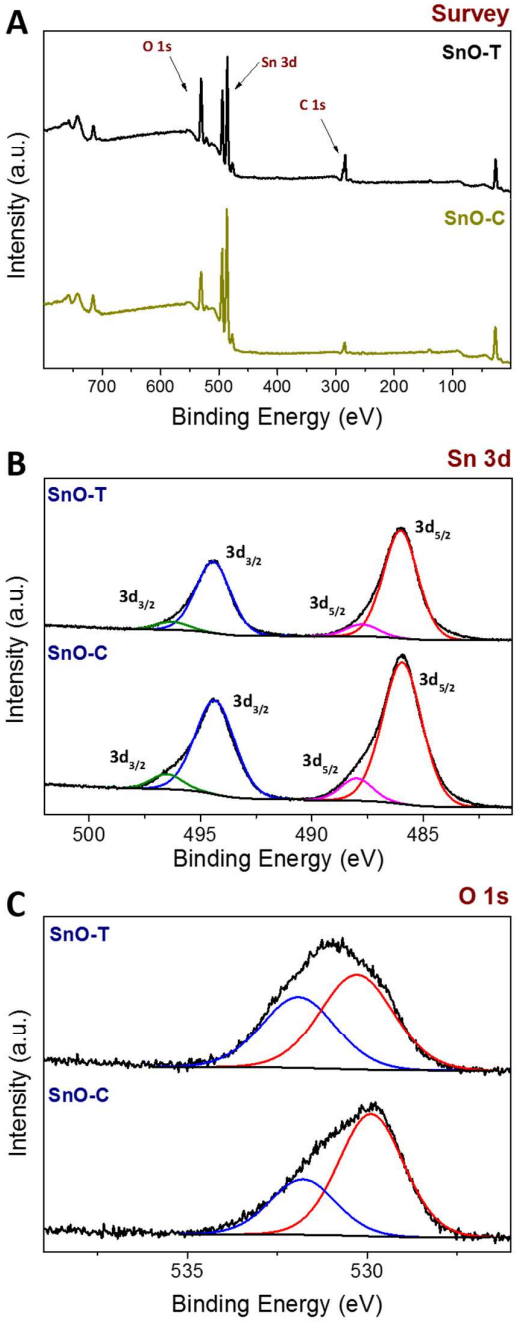

Figure 8. (A) Survey scan (top row) and (B, C) high resolution spectra of SnO.

giving one broad peak and PbO-R-T and PbO-Y-T showing the shoulder peaks alongside the main peak. Two signals of almost equal intensity were however obtained in the O 1s spectrum of PbO-Y-T, further affirming the speculation of a second chemical environment present from the Pb 4f spectrum. Likewise from the Pb 4f spectra, O 1s signals of thermally-prepared lead oxides are at marginally lower binging energies than the chemically-prepared ones.

XPS spectra of the two tin oxides are illustrated in Figure 8, with the signal positions tabulated in Table 1 as well. Two sets of spin-orbit coupling peaks representing the Sn 3d sub-level were observed in both materials, with a spin-orbit splitting of about 8.4–8.5 eV. This value corresponds to those obtained in earlier studies, justifying that the metals existed as Sn^{2+} in the samples.[54,55] The more prominent $3d_{5/2}$ peaks were recorded at 486.0 and 485.9 eV for SnO-T and SnO-C respectively. These peak positions correspond closely to literature, at which the $3d_{5/2}$ peaks were generated at about 485.7–486.5.[53,55] Both synthesis methods appear to form almost identical tin oxides, as exemplified by the comparable positions of the Sn $3d_{5/2}$ peaks. On the other hand, the high-resolution O 1s spectra (Figure 8C) of the two samples were deconvoluted into two well-defined peaks between 530 and 532 eV. Comparable intensities of the two O 1s peaks for both samples suggest a strong presence of oxygen in a different chemical environment, despite the majority still existing as Sn–O.

Table 1. Spin-orbit coupling peaks and splitting for PbO and SnO.

	Pb $4f_{5/2}$	Pb $4f_{7/2}$	δ	O 1s
PbO-R-C	142.9	138.1	4.8	530.1
PbO-R-T	142.4	137.5	4.9	529.7 (sh. 528.7)
PbO-Y-C	143.1, 145.4	138.2, 140.5	4.9	530.5, 532.4
PbO-Y-T	142.2	137.3	4.9	529.4 (sh. 527.4)
	Sn $3d_{3/2}$	**Sn $3d_{5/2}$**	**δ**	**O 1s**
SnO-T	494.4, 496.3	486.0, 487.8	8.4–8.5	530.3, 531.9
SnO-C	494.4, 496.5	485.9, 488.0	8.5	529.9, 531.8

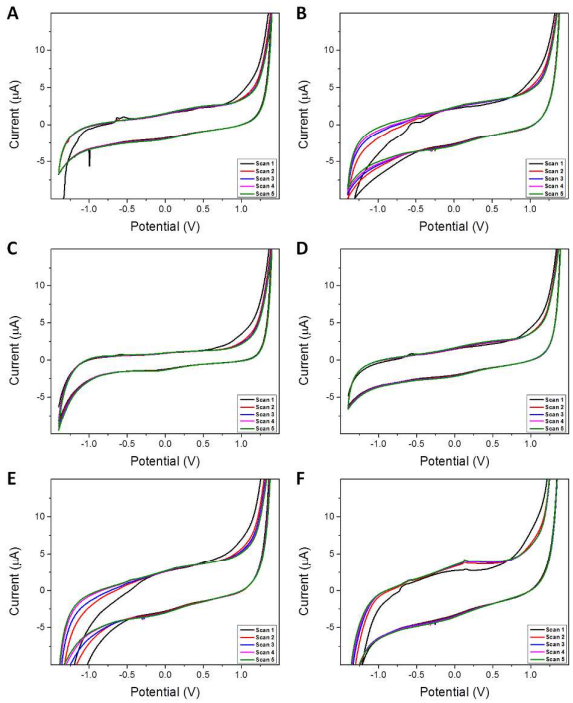

Figure 9. Cyclic voltammograms of (A) PbO-R-C, (B) PbO-R-T, (C) PbO-Y-C, (D) PbO-Y-T, (E) SnO-T and (F) SnO-C in the anodic direction in PBS background electrolyte (50 mM, pH 7.2). Scan rate: 100 mV s^{-1}.

Surface areas of all samples were measured using BET. Generally, samples prepared by thermal decomposition had larger surface compared to samples prepared by the chemical route. The obtained surface areas for lead (II) oxides were 0.352 m^2/g for PbO-R-C, 1.146 m^2/g for PbO-R-T 0.622m^2/g for PbO-Y-C and 0.731 m^2/g for PbO-Y-T. The biggest difference was found for tin (II) oxides: while sample SnO-C had surface 0.773 m^2/g, SnO-T had 11.933 m^2/g. Obtained results are in good agreement to observed SEM micrographs.

Electrochemical studies were subsequently performed on the materials following the characterisation. Inherent electrochemistry was first carried out to identify the innate oxidation and reduction signals of the materials against a background electrolyte, which is phosphate buffer solution in this work. As exemplified in Figure 9, no significant oxidation peaks were observed for the materials other than slight shoulder peaks at near –0.5 and +0.2 to +0.5 V in most of them. Similarly, broad and shallow reduction peaks were obtained at about 0 to –0.2 V for the materials. The unobvious inherent electrochemistry hence reveals the absence of oxidisable or reducible species in the oxide materials.

This fact was also proved by another experiment, where oxides were cycled 10 times in the potential range 0 V to +1.3 V. After the tenth cycle powder was analyzed by XRD for samples PbO-R-T, PbO-Y-T and SnO-T which has larger surface area compare to samples prepared by chemical reactions (Figure S1). Results confirmed that PbO samples were not oxidized up to 1.3 V. In the case of SnO-T sample were also detected traces of SnO_2. XRD confirm presence of PbO and SnO, with phosphate impurities originating from buffer reaction with PbO forming $Pb_{10}(PO_4)_6(OH)_2$. These experiments confirm the stability of both oxides which is important for possible industrial use.

Heterogeneous electron transfer (HET) rates of the various materials were investigated next using potassium ferro/ferricyanide, a surface-sensitive redox probe. Surfaces modified with oxides including PbO-R-C, PbO-Y-C, PbO-Y-T and SnO-C generated larger currents than bare glassy carbon surface, as displayed in Figure 10A, deeming these surfaces more sensitive and responsive to HET. The values of HET can be evaluated using the Nicholson's method, and is inversely related to the peak-to-peak separation (ΔE_{p-p}) where a smaller ΔE_{p-p} corresponds to a faster HET. Figure 10B shows the ΔE_{p-p} for the oxide materials and how they fare against the bare GC surface. Amongst the six materials, ΔE_{p-p} obtained for the two yellow forms of PbO and two SnO (from 348 to 360 mV) are

smaller than that of bare GC surface (378 mV). This is indicative of the faster HET rates achieved when the GC surface is modified with these oxide materials. Between the two types of metal oxides, tin oxide seemed to perform slightly better than lead oxide, where the HET constants for the respective best-performing material, SnO-C and PbO-Y-T are calculated to be 1.48×10^{-4} cm s^{-1} and 1.25×10^{-4} cm s^{-1}. However, a further comparison between the two forms of PbO concludes that the yellow form is more competent in enhancing heterogeneous electron transfers than the red form, as the ΔE_{p-p} values for the latter exceeded 400 mV.

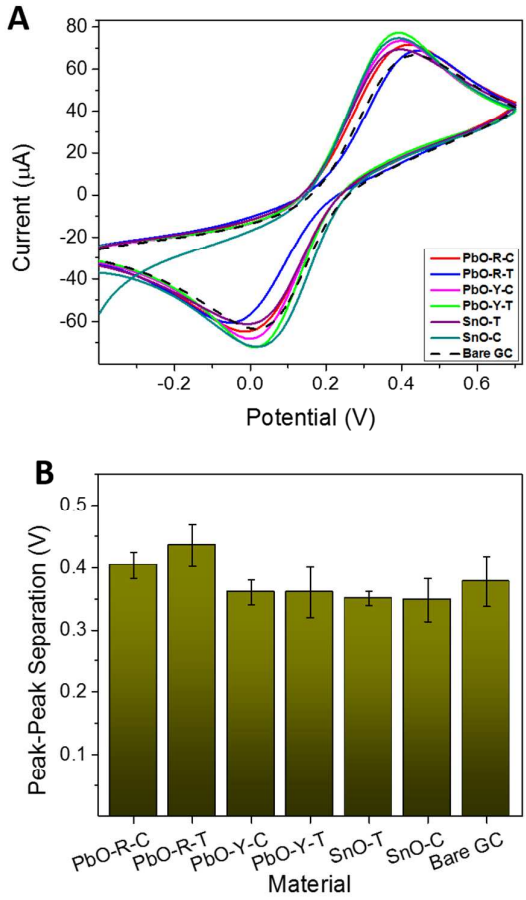

Figure 10. (A) Cyclic voltammograms of oxide materials against bare GC surface in 10 mM potassium ferro/ferricyanide and (B) their respective peak-to-peak separation. Scan rate: 100 mV s^{-1}.

The electrocatalytic potentials of the oxide materials were explored using hydrogen evolution reaction next. Figure 11A shows the cyclic voltammetric profiles of the HER scans, and the evolution of hydrogen began earliest for SnO-T and SnO-C among the six oxide materials, at around –0.8 and –0.9 V respectively. As for the lead oxides, the onset potentials of the two yellow PbO occurred at about –1.2 V, but that of the red PbO could not be accurately detected due to the presence of a reduction signal. The reduction signals present may be attributed to other species in the electrolyte such as oxygen, as well as the inherent reduction of the materials. As such, this results in a masking of the electrocatalytic abilities of the red lead oxides. While the performances of the oxides remain inferior to Pt/C which displayed an onset potential of around –0.1 V, they were able to outperform the bare GC surface. This relatively promising electrocatalytic behaviour is also supported by prior studies which discovered potential electrocatalysts such as transition metal dichalcogenides (TMDs) and mixed oxides despite inferiority against the Pt/C material.[17,19]

Tafel values were subsequently evaluated as a second parameter, as demonstrated in Figure 11B. Among the six oxides, PbO-R-T and PbO-Y-T generated the smallest Tafel slope values of 122 and 129 mV/dec respectively, in spite of the larger overpotentials required than the tin oxides. Tafel

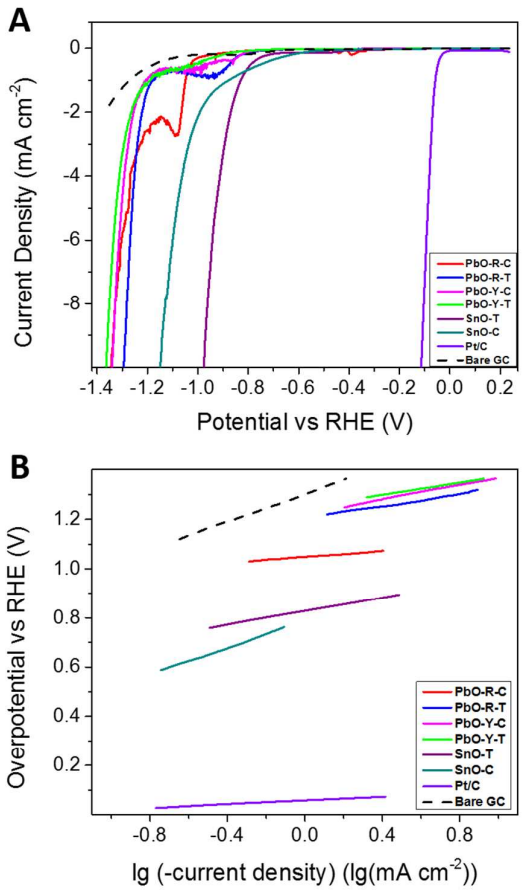

Figure 11. (A) Linear sweep voltammograms of hydrogen evolution and (B) Tafel slopes of oxide materials against platinum and bare GC surfaces. Conditions: 0.5 M sulfuric acid, scan rate 2 mV s^{-1}.

values of about 140 mV/dec were attained for PbO-Y-C and SnO-T, and slightly more than 200 mV/dec for the remaining two oxides (PbO-R-C and SnO-C). Although a wide range of Tafel slope values which are significantly larger than the value of Pt/C (~30 mV/dec) were obtained for the oxides, these values are undoubtedly smaller than that of the bare GC surface (~300 mV/dec).

Comparisons of the various parameters have shown that although these oxides might not be promising replacements for Pt/C, their results evidently demonstrated enhanced electrocatalytic behaviour and suggested presence of electrocatalytic activity when assessed against the bare GC surface; SnO-T was the best-performing oxide in particular. While the yellow PbO displayed better electrocatalytic behaviour than their red counterparts, the thermally-prepared PbO is more electrocatalytic than the chemically-prepared one. These observations can be attributed to the structures of the materials, where the yellow lead oxides exist as layered sheets compared to the huge pebble-like particles of PbO-R-C and the thermally-prepared lead oxides were broken down into smaller particles, increasing the surface area for catalysis in both scenarios. This reason also justifies the HER results between the two tin oxides, where the mesh-like SnO-T demonstrated better electrocatalytic properties than SnO-C which comprised of large blocks. A noteworthy mention is the deviations in electrocatalytic potentials when different synthesis routes were used.

Finally, oxygen reduction was performed in alkaline medium to evaluate the electrocatalytic properties of the oxide materials. Distinct reduction peaks at about –0.4 V were observed when the electrodes were modified with tin oxides, as displayed in Figure 12A. These peaks occurred slightly earlier than the bare GC surface, indicating that the tin oxides possess electrocatalytic abilities. Dashed curves in Figure 12A denote the control study, where oxygen reduction reaction was performed in the same electrolyte, but purged with nitrogen. This is carried out to remove any saturated oxygen in the potassium hydroxide solution, and the absence of signals in these curves have affirmed that the reduction signals observed in the continuous curves signify the reduction of oxygen. This comparison suggests promising catalytic abilities of the SnO for ORR. Between the two tin oxides, onset of oxygen reduction took place earlier for SnO-C (Figure 12B) with a larger current value achieved as compared to SnO-T. On the contrary, surfaces modified with lead oxides did not show clear oxygen reduction signals. Instead, only slight waves were seen for three lead oxides (PbO-R-C, PbO-Y-C, PbO-Y-T) at –0.45 V, while PbO-R-T gave a broad signal at around –0.6 V. It is hence evident than tin oxides exhibit better electrocatalytic behaviour than lead oxides for the reduction of oxygen.

Conclusions

Electrochemical studies were performed on four lead oxides and two tin oxides following their syntheses and characterisations. Tin oxide proved to be a more outstanding material for heterogeneous electron transfer and hydrogen evolution than lead oxide. Out of the four lead oxides (tetragonal and orthorhombic prepared by thermal decomposition and crystallization from solution), the orthorhombic form prepared by thermal decomposition exhibited better electrochemical behaviours. This owes largely to the structures and surface compositions of the materials, where the increased surface area played a vital role in enhancing the electrochemical abilities of the oxides. Electrochemical information on these oxides undeniably paves the way for more promising catalytic materials in the future as it is highly possible to enhance the behaviour of materials by modifying their structures or synthesis pathways to suit the requirements of a potential catalyst.

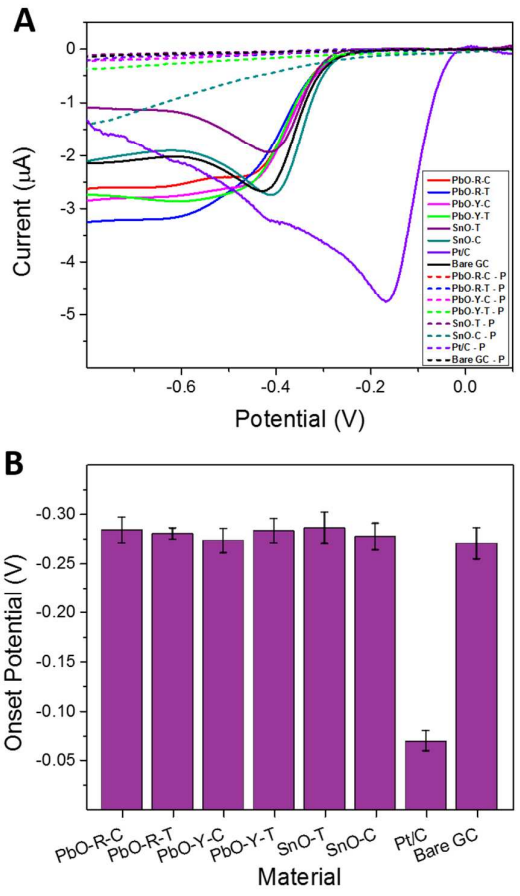

Figure 12. (A) Linear sweep voltammograms of oxygen reduction and (B) onset potentials of oxide materials against platinum and bare GC surfaces. Conditions: 0.1 M potassium hydroxide (continuous lines in Figure 7A) and 0.1 M potassium hydroxide purged in nitrogen (dashed lines in Figure 7A), scan rate 5 mV s^{-1}.

Acknowledgements

M. P. acknowledges Singapore Ministry of Education Academic Research Fund AcRF Tier 1 (2013-T1-001-014, RGT1/13) for the funding support. Z.S. and O.J. were supported by Specific University Research (MSMT No. 20/2015) and Czech Science Foundation (GACR No. 13-17538S and 15-07912S).

Notes and references

1 H. Jiang, J. Ma and C. Li, *Adv. Mater.*, 2012, **24**, 4197.
2 X. Lang, A. Hirata, T. Fujita and M. Chen, *Nat. Nanotech.*, 2011, **6**, 232.
3 S. Jeong and J. Moon, *J. Mater. Chem.*, 2012, **22**, 1243.

4 X. Xia, Y. Zhang, D. Chao, C. Guan, Y. Zhang, L. Li, X. Ge, I. M. Bacho, J. Tu and H. J. Fan, *Nanoscale*, 2014, **6**, 5008.
5 Y. Jiang, P. Wang, X. Zang, Y. Yang, A. Kozinda and L. Lin, *Nano Lett.*, 2013, **13**, 3524.
6 M. Liu, R. Liu and W. Chen, *Biosens. Bioelectron.*, 2013, **45**, 206.
7 X. Liu, H. Jia, Z. Sun, H. Chen, P. Xu and P. Du, *Electrochem. Commun.*, 2014, **46**, 1.
8 A. Umar, *Nanoscale Res. Lett.*, 2009, **4**, 1004.
9 M. A. Ibrahem, H.-Y. Wei, M.-H. Tsai, K.-C. Ho, J.-J. Shyue and C. W. Chu, *Sol. Energy Mater. Sol. Cells*, 2013, **108**, 156.
10 M. Jacobs, S. Muthukumar, A. P. Selvam, J. E. Craven and S. Prasad, *Biosens. Bioelectron.*, 2014, **55**, 7.
11 X. You, J. H. Pikul, W. P. King and J. J. Pak, *Appl. Phys. Lett.*, 2013, **102**, 253103.
12 D. Ling and T. Hyeon, *Small*, 2013, **9**, 1450.
13 S. Hu, M. R. Shaner, J. A. Beardslee, M. Lichterman, B. S. Brunschwig and N. S. Lewis, *Science*, 2014, **344**, 1005.
14 K. X. Wang, Z. Yu, V. Liu, M. L. Brongersma, T. F. Jaramillo and S. Fan, *ACS Photonics*, 2014, **1**, 235.
15 S. Berger, A. Ghicov, Y. C. Nah and P. Schmuki, *Langmuir*, 2009, **25**, 4841.
16 F. Lin, D. T. Gillaspie, A. C. Dillon, R. M. Richards and C. Engtrakul, *Thin Solid Films*, 2013, **527**, 26.
17 Z. Wu, B. Fang, A. Bonakdarpour, A. Sun, D. P. Wilkinson and D. Wang, *Appl. Catal, B*, 2012, **125**, 59.
18 M. Chhowalla, H. S. Shin, G. Eda, L.-J. Li, K. P. Loh and H. Zhang, *Nat. Chem.*, 2013, **5**, 263.
19 Y. Liang, H. Wang, J. Zhou, Y. Li, J. Wang, T. Regier and H. Dai, *J. Am. Chem. Soc.*, 2012, **134**, 3517.
20 C. S. Lim, C. K. Chua, Z. Sofer, O. Jankovský and M. Pumera, *Chem. Mater.*, 2014, **26**, 4130.
21 C. K. Chua, Z. Sofer, O. Jankovský and M. Pumera, *ChemPhysChem*, 2015, **16**, 769.
22 M. Batzill and U. Diebold, *Prog. Surf. Sci.*, 2005, **79**, 47.
23 J. Pannetier and G. Denes, *Acta Cryst.*, 1980, **B36**, 2763.
24 X. Q. Pan and L. Fu, *J. Electroceram.*, 2001, **7**, 35.
25 Y. Ogo, H. Hiramatsu, K. Nomura, H. Yanagi, T. Kamiya, M. Hirano and H. Hosono, *Appl. Phys. Lett.*, 2008, **93**, 032113.
26 Z. R. Dai, Z. W. Pan and Z. L. Wang, *J. Am. Chem. Soc.*, 2002, **124**, 8673.
27 W. Yue, S. Yang, Y. Ren and X. Yang, *Electrochimica Acta*, 2013, **92**, 412.
28 F. Kazumi, N. Chizuko, M. Keizo and M. Shunmei, *Bull. Chem. Soc. Jpn.*, 1990, **63**, 2718.
29 M. S. El-Shall, W. Slack, W. Vann, D. Kane and D. Hanley, *J. Phys. Chem.*, 1994, **98**, 3067.
30 Z. Han, N. Guo, F. Li, W. Zhang, H. Zhao and Y. Qian, *Mater. Lett.*, 2001, **48**, 99.
31 W. J. Moore Jr. and L. Pauling, *J. Am. Chem. Soc.*, 1941, **63**, 1392.
32 R. G. Dickinson and J. B. Friauf, *J. Am. Chem. Soc.*, 1924, **46**, 2457.
33 G. Trinquier and R. Hoffmann, *J. Phys. Chem.*, 1984, **88**, 6696.
34 E. A. Peretti, *J. Am. Ceram. Soc.*, 1957, **40**, 171.
35 B. Dickens, *J. Inorg. Nucl. Chem.*, 1965, **27**, 1495.
36 M. Simon, R. A. Ford, A. R. Franklin, S. P. Grabowski, B. Menser, G. Much, A. Nascetti, M. Overdick, M. J. Powell and D. U. Wiechert, *IEEE Trans. Nucl. Sci.*, 2005, **52**, 2035.
37 H. Karami, M. A. Karimi, S. Haghdar, A. Sadeghi, R. Mir-Ghasemi and S. Mahdi-Khani, *Mater. Chem. Phys.*, 2008, **108**, 337.
38 S.-E. Park and J.-S. Chang, *Appl. Catal. A*, 1992, **85**, 117.
39 H. Li, X. Huang and L. Chen, *J. Power Sources*, 1999, **81–82**, 340-345.
40 a) H. Y. Peng, H. Y. Chen, W. S. Li, S. J. Hu, H. Li, J. M. Nan and Z. H. Xu, *J. Power Sources*, 2007, **168**, 105-109; b) A. Oury, A. Kirchev, Y. Bultel and E. Chainet, *Electrochim. Acta*, 2012, **71**, 140-149.
41 S. Li, W. Yang, M. Chen, J. Gao, J. Kang and Y. Qi, *Mater. Chem. Phys.*, 2005, **90**, 262-269.
39 A. Umar, *Nanoscale Res. Lett.*, 2009, **4**, 1004.
40 M. A. Ibrahem, H.-Y. Wei, M.-H. Tsai, K.-C. Ho, J.-J. Shyue and C. W. Chu, *Sol. Energy Mater. Sol. Cells*, 2013, **108**, 156.
[44] J. C. Manifacier, L. Szepessy, J. F. Bresse, M. Perotin and R. Stuck, *Mater. Res. Bull.*, 1979, **14**, 163-175.
[45] Y. Han, X. Wu, Y. Ma, L. Gong, F. Qu and H. Fan, *CrystEngComm*, 2011, **13**, 3506-3510.
[46] J. Liu, T. Luo, S. Mouli T, F. Meng, B. Sun, M. Li and J. Liu, *Chem. Commun.*, 2010, **46**, 472-474.
41 C. Pirovano, M. S. Islam, R.-N. Vannier, G. Nowogrocki and G. Mairesse, *Solid State Ionics*, 2001, **140**, 115.
42 D. A. Grisafe and W. B. White, *Am. Mineral.*, 1964, **49**, 1184.
43 J.-R. Gavarri and D. Weigel, *J. Solid State Chem.*, 1975, **13**, 252.
44 C. A. Sorrell, *J. Am. Ceram. Soc.*, 1973, **56**, 613.
45 H. F. McMurdie, M. Morris, E. Evans, B. Paretzkin, W. Wong-Ng and Y. Zhang, *Powder Diffr.*, 1987, **2**, 41.
46 J. M. Thomas and M. J. Tricker, *J. Chem. Soc. Faraday Trans. II*, 1975, **71**, 329.
47 J. A. Taylor, G. M. Lancaster and J. W. Rabalais, *J. Electron Spectro. Relat. Phenom.*, 1978, **13**, 435.
48 J. C. Fuggle and M. Mårtensson, *J. Electron Spectrosc. Relat. Phenom.*, 1980, **21**, 275.
49 J.-M. Themlin, M. Chtaïb, L. Henrard, P. Lambin, J. Darville and J.-M. Gilles, *Phys. Rev. B*, 1992, **46**, 2460.